Spatial evolution of a quasi-two-dimensional Kármán vortex street subjected to a strong uniform magnetic field

Ahmad H. A. Hamid, Wisam K. Hussam, Alban Pothérat, and Gregory J. Sheard

---

Articles you may be interested in

Three-dimensional numerical simulations of magnetohydrodynamic flow around a confined circular cylinder under low, moderate, and strong magnetic fields
Phys. Fluids **25**, 074102 (2013); 10.1063/1.4811398

Three-dimensional transition of vortex shedding flow around a circular cylinder at right and oblique attacks
Phys. Fluids **25**, 014105 (2013); 10.1063/1.4788934

A numerical study of the laminar necklace vortex system and its effect on the wake for a circular cylinder
Phys. Fluids **24**, 073602 (2012); 10.1063/1.4731291

Optimal transient disturbances behind a circular cylinder in a quasi-two-dimensional magnetohydrodynamic duct flow
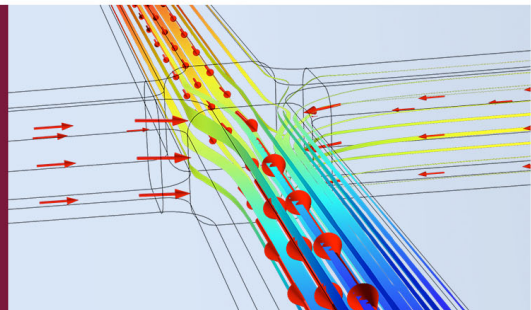Phys. Fluids **24**, 024105 (2012); 10.1063/1.3686809

Universal wake structures of Kármán vortex streets in two-dimensional flows
Phys. Fluids **17**, 073601 (2005); 10.1063/1.1943469

Spatial evolution of a quasi-two-dimensional Kármán vortex street subjected to a strong uniform magnetic field

Ahmad H. A. Hamid,[1,2] Wisam K. Hussam,[1] Alban Pothérat,[3] and Gregory J. Sheard[1,a]

[1]*The Sheard Lab, Department of Mechanical and Aerospace Engineering, Monash University, Victoria 3800, Australia*
[2]*Faculty of Mechanical Engineering, Universiti Teknologi MARA, 40450 Selangor, Malaysia*
[3]*Applied Mathematics Research Centre, Coventry University, Priory Street, Coventry CV15FB, United Kingdom*

A vortex decay model for predicting spatial evolution of peak vorticity in a wake behind a cylinder is presented. For wake vortices in the stable region behind the formation region, results have shown that the presented model has a good capability of predicting spatial evolution of peak vorticity within an advecting vortex across $0.1 \leq \beta \leq 0.4$, $500 \leq H \leq 5000$, and $1500 \leq Re_L \leq 8250$. The model is also generalized to predict the decay behaviour of wake vortices in a class of quasi-two-dimensional magnetohydrodynamic duct flows. Comparison with published data demonstrates remarkable consistency. © *2015 AIP Publishing LLC.*
[http://dx.doi.org/10.1063/1.4919906]

I. INTRODUCTION

The development of the cooling blanket for magneto-confinement fusion reactors has received attention due to its importance in controlling the core temperature. It is known that magnetohydrodynamic (MHD) effects serve to reduce the thermal-hydraulic performance by greatly increasing the pressure drop and reducing the heat transfer coefficient through laminarization of the flow of liquid metal coolant through ducts within the blanket. The stabilizing effect stems from the additional damping in the form of Joule dissipation due to the interaction between induced electric currents and the applied magnetic field.[1–3] Hence, a challenge for researchers has been to enhance heat transfer from a duct side wall via modification of the mean velocity profile, i.e., generating vortical velocity fields. The vortex motion induces a significant velocity component in the direction orthogonal to the magnetic field and thus, improves convective heat transport in this direction. The vortices can be generated by means of obstruction such as cylinders,[4–8] thin strips,[9] and wall protrusions.[10] The obstruction may also take a non-solid form, such as fringing magnetic fields.[11–14] When a conducting fluid passes the localized zone of applied magnetic field, referred to as a *magnetic obstacle*, shear layers around the obstacle develop into time periodic vortical structures. Previous research has also shown that inhomogeneous wall conductivity may generate unstable internal shear layers and leads to a time-dependent flow similar to the wake produced behind bluff bodies.[15] Current injection has been used as a source of vorticity too, as in the experiments of Sommeria,[16] Alboussière, Uspenski, and Moreau,[17] and Pothérat and Klein.[18]

In the present investigation, the vortices are generated using a circular cylinder aligned with the magnetic field. In the absence of a magnetic field, flow around a circular cylinder is steady, attached, and nearly symmetrical upstream and downstream at very low Reynolds numbers. At $Re \approx 6$, the upstream-downstream symmetry breaks as flow around the cylinder separates, creating a pair of vortices attached to the leeward side of the cylinder.[19] These eddies elongate as Re increases, ultimately succumbing to the first instability at $Re \approx 47$,[20] where a regular pattern of vortices known as

---

a)Electronic mail: Greg.Sheard@monash.edu

27, 053602-1

the Kármán vortex street appears.[21] For Reynolds numbers $50 \lesssim Re \lesssim 150$, wake vortices are shed in a half-wavelength staggered array. Vortices in viscous fluids are always subjected to a dissipative effect due to viscosity, which results in the gradual decay of their strength.

The evolution and the decay of wake vortices in normal hydrodynamic (HD) flow have received considerable attention in previous studies, for example, in Refs. 22 and 23. The solution to the vortex strength under the viscous effect is described by the Lamb–Oseen vortex model, where the peak vorticity decreases inversely with time.[23] However, when the fluid is electrically conducting and subjected to a strong magnetic field, the decay of wake vortices perpendicular to the field is accelerated via Joule dissipation (due to the Lorentz forces induced by the magnetic field)[24] and will experience exponential decay.[16] This fact was confirmed by the experimental investigation of Frank, Barleon, and Müller,[25] where they measured the vorticity of the cylinder wake at four different streamwise locations. The result revealed that the vortex intensity decayed much faster at Hartmann number $Ha = 1200$ than at $Ha = 500$ as they advected downstream. They conclude that the vortex energy dissipates by Hartmann braking rather than by cascading down towards smaller scales, which is a prominent feature of quasi-two-dimensional (quasi-2D) MHD flow as compared to pure hydrodynamic flow. When the Hartmann number is increased above a critical value, the shedding is completely inhibited.[8,26] However, it has been found that the orientation of the magnetic field plays an important role in the decay of wake vorticity. Numerical investigation of three-dimensional (3D) MHD flows[27] reveals that the vortices whose axes are aligned with the magnetic field persist far downstream, whereas vortices perpendicular to the magnetic field are rapidly damped. This observation is in agreement with the previous experimental investigation by Branover, Eidelman, and Nagorny,[9] where the intensity of velocity fluctuation is preserved for an extended period of time when the vortices are aligned with the magnetic field but get suppressed when they are perpendicular to the magnetic field. The decay rate of vorticity is also influenced by the conductivity of the Hartmann walls. For perfectly insulating walls, the characteristic decay time of vorticity depends on Hartmann braking with a scale proportional to Re/Ha.[15] A numerical investigation by Hussam, Thompson, and Sheard[8] found that for high Reynolds and Hartmann numbers, the viscous diffusion is negligible, and the decay of peak vorticity magnitude of an individual wake vortex is described by the Hartmann friction term only, i.e., Re/Ha, as suggested by theory.

In summary, considerable research has been conducted into the behaviour of wake vortices, with and without a magnetic field. However, little is known about the decaying core vorticity behaviour. In the current work, the decay of wake vortices under various flow parameters is quantitatively analyzed. The aim is to devise a model describing the decay behaviour of the peak vorticity within wake vortices behind a cylinder under the influence of a strong magnetic field. The obtained model is intended to inform the employment of cylinders as a turbulence promoter, e.g., the most favourable location of an auxiliary cylinder, a downstream cylinder which acts to sustain the dying vortices by means of proximity-induced interference effects. Furthermore, physical interpretations deduced from the findings are expected to furnish valuable information for the design of efficient heat transport systems in high-magnetic-field applications.

The paper is organised as follows. The derivation of an analytical solution for the decaying line vortex in a quasi-2D MHD flow (analogous to the Lamb–Oseen solution[22,28] for non-MHD flows) is presented in Sec. II. In Sec. III, the methodology is presented, where the problem is defined and the numerical scheme and model setup are described. The numerical validation and the grid independence study are also covered in this section. The derivation and the validation of the analytical model for wake vortices are reported in Sec. IV, and the insights provided by the model are discussed in Sec. V. Section VI is dedicated to the comparison with three-dimensional numerical data, followed by conclusions in Sec. VII.

II. ANALYTICAL SOLUTION FOR VORTEX DECAY IN A QUASI-2D FLOW

In this section, the analytical solution for the decaying line vortex is devised to gain fundamental understanding of the behaviour of an isolated vortex in a quasi-two-dimensional flow, which will serve as the basis for a regression fit describing the evolution of cylinder wake peak vorticity in a rectangular duct. A quasi-two-dimensional model proposed by Sommeria and Moreau[1]

(hereafter referred to as the SM82 model) has been employed in the current work. This model is derived by averaging the flow quantities along the magnetic field direction. Formally, the quasi-two-dimensional model is accurate to order $O(Ha^{-1}, N^{-1})$, where $N = \sigma B^2 a/\rho U$ is the interaction parameter, $Ha = Ba\sqrt{\sigma/\rho\nu}$ is the Hartmann number, σ, ν and ρ are electrical conductivity, kinematic viscosity, and density of the liquid metal, respectively, U is a typical velocity, B is the imposed magnetic field, and a is channel depth in the magnetic field (out-of-plane) direction. Under this quasi-two-dimensional model, the magnetohydrodynamic equations of continuity and momentum reduce to

$$\hat{\nabla} \cdot \hat{\mathbf{u}}_\perp = 0 \tag{1}$$

and

$$\frac{\partial \hat{\mathbf{u}}_\perp}{\partial \hat{t}} = -(\hat{\mathbf{u}}_\perp \cdot \hat{\nabla})\hat{\mathbf{u}}_\perp - \frac{1}{\rho}\hat{\nabla}\hat{p} + \nu\hat{\nabla}^2\hat{\mathbf{u}}_\perp - \frac{n}{t_H}\hat{\mathbf{u}}_\perp, \tag{2}$$

respectively, where $\hat{\mathbf{u}}_\perp$ and $\hat{p}_\perp$ are the respective velocity and pressure fields, projected onto a plane orthogonal to the magnetic field, $\hat{t}$ is time, $\hat{\nabla}$ is the gradient operator, and $t_H = (a/B)\sqrt{\rho/\sigma\nu}$ is the Hartmann damping time.[29] Here, $n = 2$ is the number of Hartmann layers.

Reference 29 explains that quasi-two-dimensionality is achieved when the time scale for the Lorenz force to act to diffuse momentum of a structure of size $l_\perp$ along magnetic field lines over length $l_\parallel$, $\tau_{2D} = (\rho/\sigma B^2)l_\parallel^2/l_\perp^2$, is shorter than the time scales for viscous diffusion in the perpendicular and parallel planes ($\tau_\nu^\perp = l_\perp^2/\nu$ and $\tau_\nu^\parallel = l_\parallel^2/\nu$, respectively) and the inertia time scale $\tau_U = l_\perp/U$. Taking $l_\parallel = a$, these three conditions can be used, respectively, to obtain limiting length scales under the model, $l_\perp/a > Ha^{-1/2}$, $l_\perp/a > Ha^{-1}$, and $l_\perp/a > N^{-1/3}$. The second condition is always satisfied under the first condition for $Ha > 1$.

From Hussam, Thompson, and Sheard,[8] the curl of Eq. (2) yields the quasi-two-dimensional vorticity transport equation for an incompressible flow of an electrically conducting fluid between two plates subjected to a uniform strong magnetic field in the out-of-plane direction, given in dimensional form as

$$\frac{D\hat{\xi}_\perp}{D\hat{t}} = \nu\hat{\nabla}^2\hat{\xi}_\perp - \frac{2}{t_H}\hat{\xi}_\perp, \tag{3}$$

where $\hat{\xi}_\perp$ is vorticity and $D/D\hat{t}$ the material derivative. Therefore, an advecting packet of vorticity will be subjected to both a diffusion process acting to smooth out the vorticity field and an exponential damping due to the quasi-two-dimensional friction term. By scaling the length by a, the time by a^2/ν and the vorticity by ν/a^2, the transport equation can be written as

$$\frac{D\xi_\perp}{Dt} = \nabla^2\xi_\perp - 2Ha\,\xi_\perp, \tag{4}$$

where $\xi_\perp$, t, and ∇ are dimensionless counterparts to $\hat{\xi}_\perp$, $\hat{t}$, and $\hat{\nabla}$, respectively. We first consider a solution for the decay of a quasi-2D vortex located at the frame origin, maintaining a solely exponential decay of circulation through Hartmann braking far from the vortex, in an open quasi-two-dimensional flow. For convenience, Eq. (4) is expressed for an axisymmetric ($\partial/\partial\theta = 0$) flow in cylindrical coordinates as

$$\frac{D\xi_\perp}{Dt} = \frac{\partial^2\xi_\perp}{\partial r^2} + \frac{1}{r}\frac{\partial\xi_\perp}{\partial r} - 2Ha\,\xi_\perp, \tag{5}$$

where r is the radial coordinate and the vortex is located at $r = 0$. Recognising that radial velocity $v_r = 0$ and $\partial\xi_\perp/\partial\theta = 0$ for decaying quasi-2D vortex flow, the material derivative reduces to $\partial\xi_\perp/\partial t$, and Eq. (5) can be transformed[30] using

$$\xi_\perp(r,t) = e^{(-2Ha\,t)}\xi(r,t) \tag{6}$$

to give

$$\frac{\partial\xi}{\partial t} = \frac{\partial^2\xi}{\partial r^2} + \frac{1}{r}\frac{\partial\xi}{\partial r}. \tag{7}$$

This is precisely the vorticity transport equation for an azimuthal axisymmetric hydrodynamic flow about $r = 0$. For the case of the temporal decay of a quasi-2D vortex, conserving circulation as $r \rightarrow \infty$, the solution to this equation is exactly the Lamb–Oseen vortex solution, where the vorticity field is given by

$$\xi = \frac{\Gamma}{\pi r_c^2} e^{\left(-r^2/r_c^2\right)}. \tag{8}$$

Note that this solution is indeed independent of θ, and it can readily be shown that $v_r = 0$. Γ represents the initial amount of circulation contained in the elementary quasi-2D vortex. The vortex evolves over time $\tau = t - t_0$, where t_0 is an arbitrary initial time. Applying the transformation in Eq. (6) yields

$$\xi_\perp = \frac{\Gamma}{\pi r_c^2} e^{-r^2/r_c^2} e^{-2Ha\tau}, \tag{9}$$

and the peak vorticity is expressed by solving for $r = 0$, giving

$$\xi_{\perp,p} = \frac{\Gamma}{\pi r_c^2} e^{-2Ha\tau}. \tag{10}$$

The dimensionless core radius evolves as $r_c = \sqrt{4\tau}$ (note the absence of ν from the argument of the square root due to the non-dimensionalisation, compared to the dimensional solution).[31] Substituting to eliminate r_c and taking the time derivative yield

$$\frac{\partial \xi_{\perp,p}}{\partial \tau} = -\frac{\Gamma}{4\pi\tau} e^{-2Ha\tau} \left[2Ha + \frac{1}{\tau}\right]. \tag{11}$$

The terms in the square brackets constitute the Hartman braking and viscous contributions to the vortex decay, respectively. Equating these, substituting τ in terms of r_c and solving give a threshold core radius below which viscosity exceeds Hartman friction in reducing the peak vortex strength, $r_{c1} = \sqrt{2}Ha^{-1/2}$. The vortex core diameter is then given by $d_{c1} = 2^{3/2}Ha^{-1/2} \approx 3Ha^{-1/2}$, i.e., approximately three times the limiting scale on perpendicular flow structures under the quasi-two-dimensional model, $l_\perp/l_\parallel = Ha^{-1/2}$. Therefore, vortices whose decay is contributed significantly by viscous diffusion can exist in a quasi-two-dimensional flow under the SM82 model.

Substituting $Ha = 0$ into Eq. (10) recovers the peak vortex time history for a Lamb–Oseen vortex written here in terms of time,

$$\xi_p = \frac{\Gamma}{4\pi(t - t_0)}, \tag{12}$$

and finally, the corresponding expression for a vortex in quasi-two-dimensional flow is

$$\xi_{\perp,p} = \frac{\Gamma}{4\pi(t - t_0)} e^{-2Ha(t-t_0)}. \tag{13}$$

Equation (13) will serve as a basis for the form of the correlation function developed in this paper. It is important to note that real wake vortices experience different effects to an isolated Lamb–Oseen vortex due to the fact that wake vortices are being advected downstream and there is interaction between neighbouring vortices, which leads to mutual straining and merging among the vortices.[32,33] Furthermore, wake vortices experience a confinement effect due to the duct wall, where in high-blockage cases, the vortices shed from the wall can cause dramatic changes in the global flow behaviour and modification of the flow structure.[34] On the other hand, an isolated vortex possesses a general structure of monotonic decrease of vorticity with radial distance from a central extremum.[33] Hence, it is expected that the model being developed will be more complicated than the solutions in Eqs. (12) and (13).

Before proceeding with the analytical model, we will briefly explore the scaling condition arising from the inertial time scale,

$$l_\perp/a > N^{-1/3}, \tag{14}$$

in the context of a quasi-two-dimensional vortex. The tangential velocity profile for the vortex can be adapted from the known Lamb–Oseen solution (e.g., see Ref. 35) written in terms of initial circulation as

$$u_\theta(r,t) = \frac{\Gamma}{2\pi r}\left(1 - e^{-r^2/r_c^2}\right)e^{-2Ha\tau} \tag{15}$$

and maximum tangential velocity $u_{\theta,\max}$ as

$$u_\theta(r,t) = u_{\theta,\max}\left(1 + \frac{1}{2\alpha}\right)\frac{r_{\max}}{r}\left[1 - e^{-\alpha r^2/r_{\max}^2}\right]e^{-2Ha\tau}, \tag{16}$$

where $r_{\max} = \sqrt{\alpha}r_c(t)$ is the radius at which the tangential velocity is maximum and $\alpha = 1.256\,43$ is the Lamb–Oseen constant. Given the requirement that $N \gg 1$, the dependence of N on the reciprocal of U means that considering the maximum tangential velocity as the reference velocity is equivalent to finding the minimum local interaction parameter for a vortex. Substituting $u_{\theta,\max} = U$ and solving Eqs. (15) and (16) for U yield

$$U = \frac{\hat{\Gamma}}{\sqrt{\nu\hat{t}}}\frac{\sqrt{\alpha}}{4\pi(2\alpha + 1)}. \tag{17}$$

The interaction parameter can then be expressed as

$$N = Ha^2\left[\frac{2\pi(2\alpha + 1)}{\sqrt{\alpha}}\right]\frac{r_c}{\Gamma}. \tag{18}$$

For a Lamb–Oseen vortex, a Reynolds number based on circulation is conventionally defined as $Re_\Gamma = \hat{\Gamma}/2\pi\nu = \Gamma/2\pi$. Taking the core radius to represent the scale of a quasi-two-dimensional structure, i.e., $r_c = l_\perp/l_\parallel$, and using Eq. (18) to express Eq. (14) in terms of r_c ultimately produce

$$r_c > \left[\frac{\sqrt{\alpha}}{2\alpha + 1}\right]^{1/4}N_\Gamma^{-1/4}, \tag{19}$$

where an interaction parameter based on vortex circulation, $N_\Gamma = Ha^2/Re_\Gamma$, has been introduced. The dissipation of a quasi-two-dimensional vortex through Hartman braking will reduce Re_Γ over time, in turn increasing N_Γ, thus reducing the minimum allowable scale satisfying the quasi-two-dimensional model through Eq. (19). It follows then that if a vortex initially satisfies the quasi-two-dimensional model, it will do so throughout its lifetime.

III. NUMERICAL METHOD AND VALIDATION

The system of interest is a circular cylinder confined by a rectangular duct (Fig. 1). The axis of the cylinder is parallel to the spanwise direction and perpendicular to the flow direction. A homogeneous strong magnetic field with a strength B is imposed parallel to the cylinder axis. Under this condition, the flow is quasi-two-dimensional, and thus, the SM82 model is adopted. Its
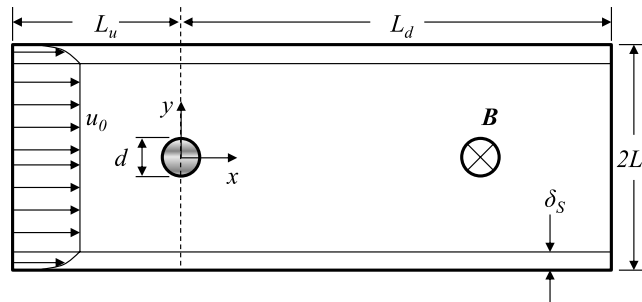

FIG. 1. Schematic diagram of the numerical domain. The shaded area indicates a cylinder of infinite extension along the out-of-plane z-axis with diameter d.

non-dimensional form reduces to

$$\nabla \cdot \mathbf{u}_\perp = 0 \tag{20}$$

and

$$\frac{\partial \mathbf{u}_\perp}{\partial t} = -(\mathbf{u}_\perp \cdot \boldsymbol{\nabla})\mathbf{u}_\perp - \nabla p_\perp + \frac{1}{Re_L}\nabla^2\mathbf{u}_\perp - \frac{H}{Re_L}\mathbf{u}_\perp, \tag{21}$$

where $Re_L = u_0 L/\nu$ is the Reynolds number based on half-channel width L and u_0 is the peak inlet velocity. Here, pressure is scaled by ρu_0^2 and time by L/u_0. All variables are expressed in their dimensionless form hereafter. The friction parameter $H = 2(L/a)^2 Ha$ is a measure of the friction term. The exact solution of Eqs. (20) and (21) satisfying the no-slip boundary conditions at the side walls for fully developed quasi-2D flow is applied at the channel inlet,[29] i.e.,

$$u_\perp(y) = \frac{\cosh\sqrt{H}}{\cosh\sqrt{H} - 1}\left(1 - \frac{\cosh\sqrt{H}y}{\cosh\sqrt{H}}\right). \tag{22}$$

At $H \gg 1$, the area-averaged velocity, u_{avg}, across the duct approaches the peak velocity u_0 (in contrast, for Poiseuille flow in a channel, $H = 0$, $u_0 = 3/2u_{avg}$). It is also convenient to define a Reynolds number based on the cylinder diameter, $Re_d = u_0 d/\nu$, and an effective Reynolds number based on mean velocity through the gaps either side of the cylinder $(2L - d)$, which simplifies to $Re'_d = 2\beta Re_L/(1 - \beta)$, where $\beta = d/2L$ is the blockage ratio. The definition of Re'_d assumes that the change in peak velocity due to cylinder blockage would be consistent with the change in area-averaged velocity. The use of different length scales in MHD cylinder wake flows is inevitable: the two-dimensional linear braking term is governed by Ha and L, whereas the structure of the cylinder wake is governed by d.[25] All boundaries are assumed to be electrically insulated.

At present, generally the SM82 model is applicable for MHD duct flows under the influence of a strong magnetic field, although some deviation from the quasi-2D behaviour can be observed in some situations, e.g., in complex geometry ducts. In the case of simple rectangular duct flows, SM82 has been verified against 3D results.[36,37] The error using this model with the three-dimensional solution has been shown to be in order of 10%.[38] However, this error is significant only in the vicinity of, and inside, the side layers. Previous work by Kanaris *et al.*[26] also provides an excellent validation of the model for MHD wakes, showing a high degree of two-dimensionalisation of cylinder wake vortices with increasing N. One can find the formulation of this model in many literatures, e.g., in Refs. 8, 38, and 39. An advanced, high-order, in-house solver based on the spectral-element method for spatial discretization is employed to simulate the flows in this study, which implements the SM82 model.[8,40,41]
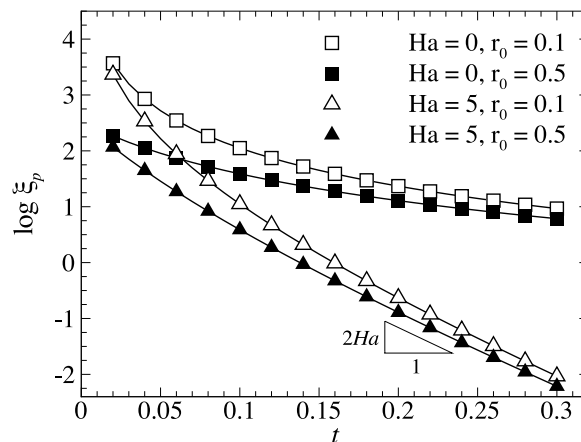

FIG. 2. Natural logarithm of peak vorticity plotted against time, for a decaying quasi-2D vortex in an open hydrodynamic flow (square symbols) and an open quasi-two-dimensional MHD flow (triangles). Open symbols show initial core radius $r_0 = 0.1$ and solid symbols show $r_0 = 0.5$. $\Gamma = 10$ for all cases. The slope of the quasi-2D curves approaches $-2Ha$ at larger times ($t \gtrsim 0.2$).
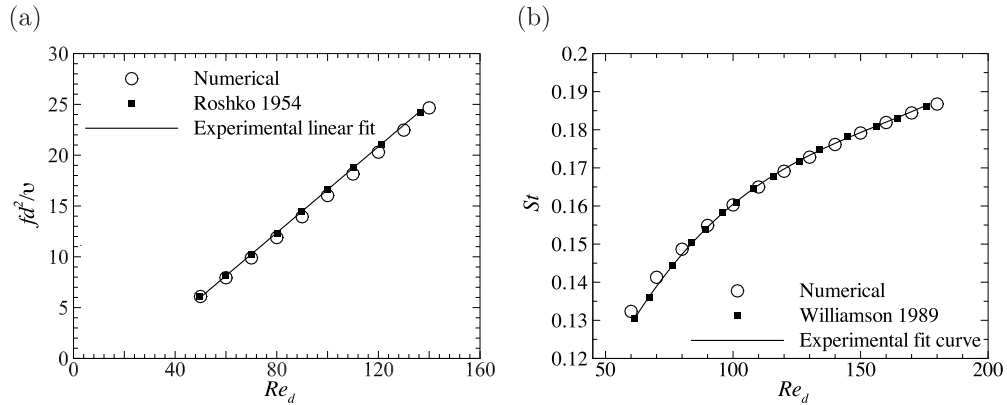
FIG. 3. (a) $f d^2/\nu$ and (b) St plotted against Re_d. Open symbols represent the present data, while solid symbols and lines represent data published in Refs. 42 and 43, respectively.

To validate the numerical scheme being used, a decaying quasi-2D vortex has been simulated and compared with the analytical solution derived in Sec. II. Simulations were carried out at various Hartmann numbers, circulations, and initial core radii. A typical comparison is shown in Fig. 2. It should be noted that the curves shown in Fig. 2 are not fittings but instead are analytical peak vorticity calculated from Eq. (13). An excellent agreement is consistently seen between the analytical and numerical results. This further serves to confirm the validity of the analytical solution obtained in Sec. II.

For further validation, the dimensionless shedding frequency data for a circular cylinder in an open hydrodynamic flow from Roshko[42] and Williamson[43] are compared with the results obtained from the present code and the agreement with the experimental data is pleasing (Figs. 3(a) and 3(b), respectively). Further validation of the code can be found in Refs. 8 and 44.

A grid independence study has been performed by varying the element polynomial degree from 4 to 10, while keeping the macro-element distribution unchanged. Meshes near the walls and the cylinder were refined to resolve the expected high gradients, especially for high-Hartmann-number cases.[45] Fig. 4 shows the spectral element discretisation of the computational domain. The pressure and viscous components of the time-averaged drag coefficient ($C_{D,p}, C_{D,\mathrm{visc}}$) and the Strouhal frequency of vortex shedding (St) were monitored, as they are known to be sensitive to the domain size and resolution. Errors relative to the case with highest resolution, $\varepsilon_P = |1 - P_{Ni}/P_{N=10}|$, were used as a monitor for each case, where P is the monitored parameter. A demanding MHD case with $Re_L = 8000$ and $H = 3750$ was chosen for the test. The results are presented in Table I and show rapid convergence when the polynomial order increases. A mesh with polynomial degree 7 achieves at most a 0.1% error while incurring an acceptable computational cost and is therefore used hereafter.
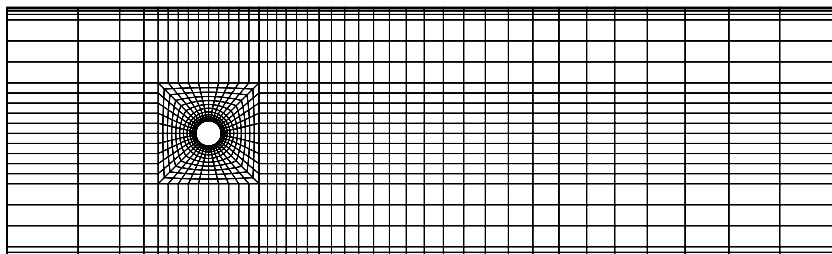

FIG. 4. Macro-element distribution. Fine resolution was placed at the proximity of cylinder surface and walls to ensure accurate representation of the thin boundary layers and the expected wake structures.

TABLE I. Grid independence study at $Re_L = 8000$ and $H = 3750$.

N_P	4	5	6	7	8	9
$\varepsilon_{C_{D,P}}$	0.0164	0.0010	0.0002	0.0002	0.0002	0.0003
$\varepsilon_{C_{D,\text{visc}}}$	0.0391	0.0024	0.0023	0.0010	0.0001	0.0000
ε_{St}	0.0036	0.0034	0.0003	0.0002	0.0001	0.0000

IV. ANALYTICAL MODEL FOR THE DECAY OF WAKE VORTICES

A. Derivation

It is observed from previous studies (and follows from the Hartmann braking term in the quasi-two-dimensional model) that increasing Hartmann number generally acts to increase the decay rate of vortices.[8] To quantify these observations, the peak vortex strength of wake vortices behind a cylinder has been recorded at different blockage ratios and a broad range of Hartmann and Reynolds numbers. The model is derived by assuming that wake vortices decay according to a law of the same form as isolated vortices, on the basis that Hartmann friction remains the dominant mechanism and that non-linear interactions act too slowly to strongly affect the vortex profile during the decay. This assumption is expected to remain valid at high N, and provided that the influence of the walls remains limited (i.e., smaller blockage ratios), we start by assuming that ξ_p and $\xi_{\perp,p}$ are of the form

$$\xi_p = \frac{a'}{t - t_0} \tag{23}$$

and

$$\xi_{\perp,p} = \frac{a'}{t - t_0} e^{-b'(t - t_0)}, \tag{24}$$

for pure hydrodynamic and magnetohydrodynamic cases, respectively, and find the values of constants by means of a regression analysis. Since the advection velocity U_ξ for the wake vortices is approximately constant,[46] we can write $t - t_0 = (x - x_0)/U_\xi$, where the cylinder is located at $x = 0$, and x_0 is the streamwise location of the virtual point vortex that the wake vortices project from. Hence, Eqs. (23) and (24) can be recast in terms of streamwise position of a wake vortex as

$$\xi_p = \frac{a}{x - x_0} \tag{25}$$

and

$$\xi_{\perp,p} = \frac{a}{x - x_0} e^{-b(x - x_0)} = \frac{a}{x - x_0} e^{-bx + c}. \tag{26}$$

While a, x_0, b, and c are constant for the Lamb–Oseen and quasi-two-dimensional vortex decay solutions (Eqs. (12) and (13), respectively), it is anticipated that these will exhibit a dependence on one or more of the control parameters (i.e., Re, H, and β) when applied to describe the decay of a transported wake vortex. The expressions for parameters a and b are obtained from simulations of hydrodynamic flow within the parameter space $0.1 \leq \beta \leq 0.4$ and $300 \leq Re_L \leq 900$. The locations and values of vorticity maxima within a single wake vortex as it advects downstream of a body are determined by searching within each spectral element for collocation points having a locally maximum vorticity magnitude, and then iterating using a Newton–Raphson method to converge on the accurate position. This approach preserves the spectral accuracy of the peak vorticity. The values of a and b were determined by curve-fitting the spatial decay of peak vortex strength for each hydrodynamic case ($H = 0$) into Eq. (25). A typical time history of peak vorticity is presented in Fig. 5.

Inspection of the data for a range of parameters revealed that a and x_0 are dependent on Reynolds numbers relating to the cylinder diameter and the blockage ratio (refer Fig. 6). It can be seen from Fig. 6(a) that parameter a increases linearly with increasing effective Reynolds number
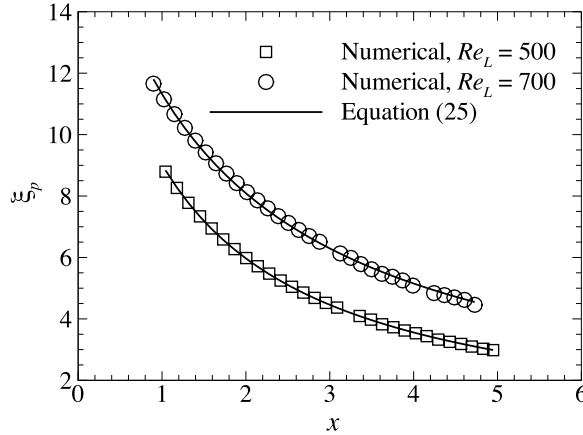
FIG. 5. Spatial evolution of peak vorticity decay for $\beta = 0.1$ and $Ha = 0$, at Reynolds numbers as indicated in the legend. Lines are least-squares fits of the data to Eq. (25).

Re'_d, and with increasing blockage ratio, the gradient decreases. Fig. 6(b) shows that parameter x_0 decreases linearly with $Re_d(1 - \beta)$, and an increase in blockage ratio produces an increase in gradient magnitude of the linear trends. The least-squares linear fits for coefficients a and x_0 take the form

$$a = M_a Re'_d - C_a \tag{27}$$

and

$$x_0 = M_{x_0} Re_d(1 - \beta) - C_{x_0}, \tag{28}$$

respectively. The slope (M) and the intercept (C) of these fits are found to vary almost linearly with β (producing coefficients of determination in the range $0.99 < r^2 < 0.994$), and the resulting relations are given in Eq. (29). Using the same approach as per the development for expressions for a and x_0 for pure hydrodynamic flow, parameters b and c are derived from the peak vorticity time history of magnetohydrodynamic cases across $0.1 \le \beta \le 0.4$, $500 \le H \le 5000$, and $1500 \le Re_L \le 8250$, where a laminar periodic shedding regime is captured throughout this parameter range. The valid upper range of Re_L is determined by both the assumptions of the SM82 model, i.e., the flow has sufficiently large perpendicular scales, in such a way that the condition of $N \gg (a/l_\perp)^3$ and $H \gg (a/l_\perp)^2$ is satisfied,[29,36] and the Hartmann layers must be laminar, i.e., the Reynolds number based on the Hartmann layer thickness $Re/H < 250$.[1] The former criterion is stricter than the latter, and by taking $N > 10$ as an indicative threshold for the applicable
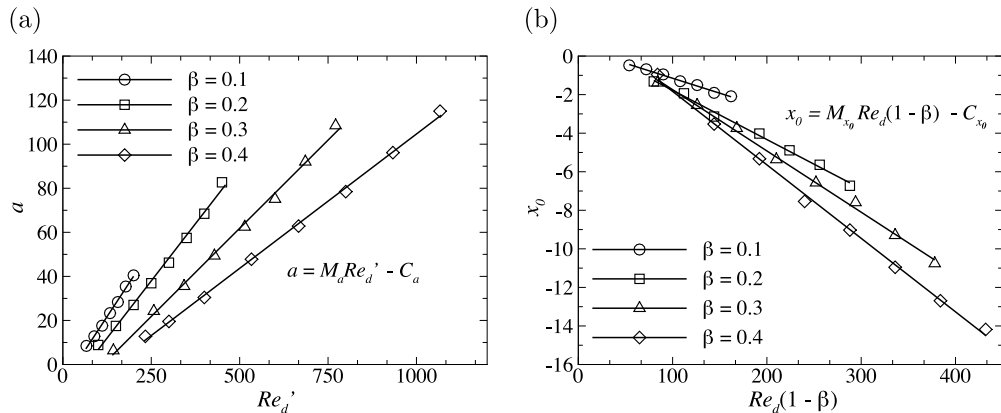

FIG. 6. Variations of parameters a and x_0 with respect to different cylinder Re and blockage ratios.

range of interaction parameters and $H = 500$, the model will break down at a Reynolds number of order $Re_L < H^2/N = 500^2/10 = 25\,000$, which is well above the maximum Re_L studied, i.e., $Re_L = 8250$. Dousset and Pothérat[38] showed that transition to a chaotic wake occurred at a critical Reynolds number in the range $6000 < Re_L < 10\,000$ for $150 < H < 1250$. While the SM82 model is well capable of reproducing the dynamics of turbulent flows as long as they remain quasi-two-dimensional and the Hartmann layer remains laminar, it breaks down if any of these assumptions are violated. If the Hartmann layer becomes turbulent, the flow may still remain quasi-two-dimensional but boundary layer friction is altered. Pothérat and Schweitzer[47] developed an alternative shallow water model which is valid in these conditions.

Regression analysis revealed that b/H exhibits a power-law dependence on Re_L, and the data exhibit a pleasingly collapse to a positive b/H shift curve of Hartmann friction term (refer Fig. 7(a)). A non-linear optimization of parameter c yields a collapse of data into a linear trend when $c/H^{0.02}$ is plotted against $\beta^{0.36}Re_L^{0.67}$, as shown in Fig. 7(b). Collecting these results, the evolution of peak vortex strength is therefore found to be given by

$$\xi_{\perp,p} = \frac{a}{x - x_0}e^{-bx+c}, \tag{29}$$

where

$$a = (-0.39\beta + 0.28)Re_d' - (34.5\beta + 4.1),$$
$$x_0 = -(0.075\beta + 0.01)Re_d(1 - \beta) + (4.3\beta - 0.15),$$
$$b = 0.90\frac{H}{Re_L^{0.974}},$$
$$c = H^{0.02}(0.004\beta^{0.36}Re_L^{0.67} - 0.1).$$

Equation (29) may be used to predict peak vorticity time history for confined hydrodynamic flows by substituting $H = 0$, which yields

$$\xi_p = \frac{(-0.39\beta + 0.28)Re_d' - (34.5\beta + 4.1)}{x + (0.075\beta + 0.01)Re_d(1 - \beta) - (4.3\beta - 0.15)}. \tag{30}$$

Further, when unbounded flow is considered, i.e., $\beta = 0$, Eq. (30) recovers the reciprocal relationship to time expected from the Lamb–Oseen vortex solution (noting that at $\beta = 0$, Re_d' reduces to Re_d), i.e.,

$$\xi_p = \frac{0.28Re_d - 4.1}{x + 0.01Re_d + 0.15} = \frac{0.28Re_d - 4.1}{U_\xi\tau}. \tag{31}$$
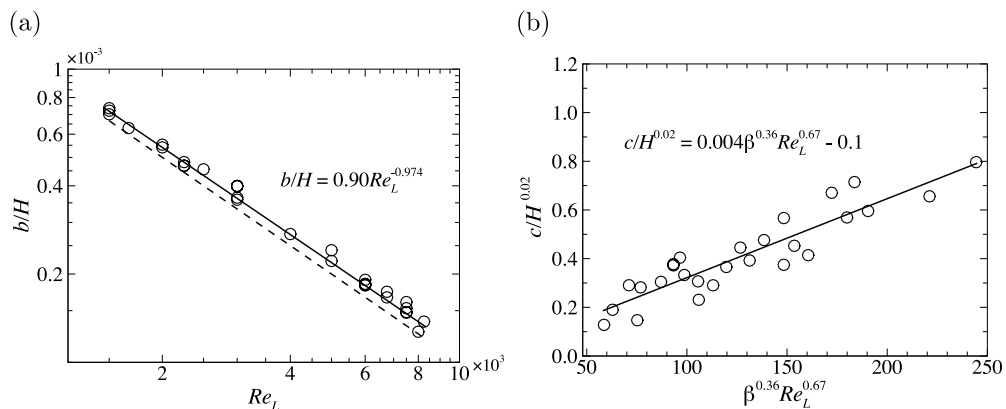

FIG. 7. (a) A plot of b/H against Re_L and (b) $c/H^{0.02}$ against $\beta^{0.36}Re_L^{0.67}$ measurements (symbols). The solid lines in (a) and (b) are a power-law fit and a linear fit, respectively, to the data adopting the equations shown, and the dashed line is the behaviour described by the Hartmann friction term (H/Re_L) for comparison.

Comparing Eq. (31) with the peak vorticity of the Lamb–Oseen vortex solution, i.e., $\xi_p = \Gamma/(4\pi\tau)$ yields

$$\Gamma = \frac{4\pi}{U_\xi}\left(0.28 - \frac{4.1}{Re_d}\right).\tag{32}$$

This equation suggests that circulation is a function of Reynolds number. Substituting $Re_d = 75$ and $U_\xi = 0.89$ (a typical wake advection velocity at this particular Reynolds number) results in $\Gamma = 3.18$, which agrees very well with the values obtained from previous numerical data, and is very close to values from experimental data of Kieft[48] (i.e., $\Gamma = 3.17$ and $\Gamma = 2.81$ from numerical and experimental data, respectively, at $Re_d = 75$). The small discrepancy between the present value and the experimental value may be due to the error in measuring velocity vectors in the experiment.[48]

B. Validation of the model

The validity of the proposed model, Eqs. (30) and (29) for HD flow and MHD flow, respectively, is examined using all the computed cases and relative standard errors (*RSEs*) are compared to assess the reliability of estimates. The RSE evaluates the residuals relative to the predicted value and is calculated as follows:[49,50]

$$\text{RSE} = \sqrt{\frac{\Sigma(\xi_{p,\text{numerical}} - \xi_{p,\text{predicted}})^2}{\Sigma\xi_{p,\text{numerical}}^2}},\tag{33}$$

where $\xi_{p,\text{numerical}}$ and $\xi_{p,\text{predicted}}$ are the peak vorticity from numerical simulations and the model predictions, respectively. The summation was performed for vortices transported over the downstream part of the domain. In general, estimates are considered statistically reliable if the *RSE* of the estimate is less than 30%.[51] Applying the model developed in this paper across the computed parameter space ($0.1 \le \beta \le 0.4$, $500 \le H \le 5000$, and $300 \le Re_L \le 8250$) results in an overall *RSE* of less than 25%, with more than 80% of the samples having a *RSE* of less than 15%. Figs. 8 and 9 represent a typical comparison of MHD cases at different Reynolds numbers and blockage ratios and overall comparison between predicted and numerically calculated peak vorticities, respectively. These figures verify that the agreement between model predictions and computed data is very good.

It should be noted that the wake vortices in laminar flow regime are generally stable, i.e., the longitudinal spacing between two successive vortices, l, is constant,[42,52,53] except at the formation region, within the parameter range currently investigated. The spacing was determined by plotting the phase-downstream distance relationships along the wake, where a typical plot is shown in Fig. 10. Here, 17 instantaneous snapshots of vorticity were taken for two periods of oscillation,
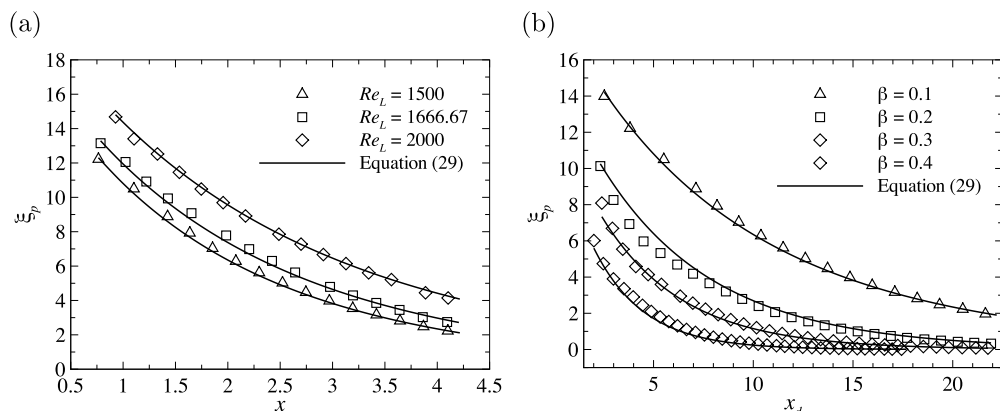

FIG. 8. Decaying peak vorticity from numerical results and prediction by Eq. (29) for (a) $H = 500$ and $\beta = 0.1$, and (b) $H = 500$ and $Re_L = 1500$.
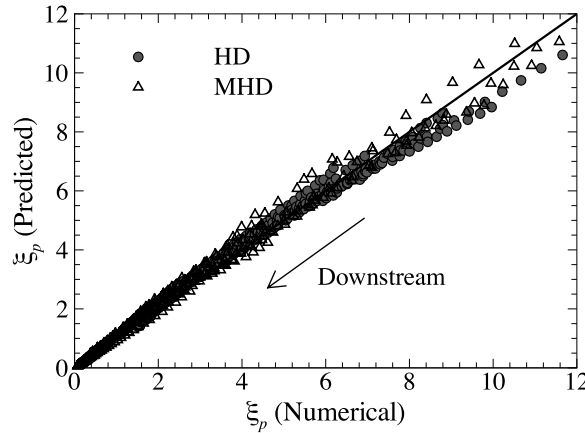
FIG. 9. Overall comparison between numerical and predicted peak vorticity. The solid line $\xi_{P,\text{predicted}} = \xi_{P,\text{numerical}}$ denotes the ideal scenario where predictions perfectly match the simulated values.

where snapshot begins at an arbitrary phase and is set to zero for comparison. The slope of the curve at any position will give the reciprocal of the longitudinal spacing of the vortices at that position. The plot shows that the longitudinal spacing becomes constant within two or three diameters downstream of the cylinder. Preceding the stable region is the formation region, where the vorticity dissipates and organises into a coherent structure in the vicinity of the cylinder.[48] This process can be further divided into three stages, namely, the accumulation of vorticity from the separated boundary layers ("vortex A" in Fig. 11(a)), the stretching of vorticity (Fig. 11(b)), and the separation of this vorticity from the boundary layer (Fig. 11(d)). The subsequent vortex ("vortex B") is also formed during the stretching of vortex A, as shown in Fig. 11(c).

Beyond the stable region, the viscous effect has become less dominant and eventually leads to vortex street breakup.[32] This unstable secondary street possesses a longer wavelength than the primary street and contains more than one dominant frequency.[15] These two regions (the formation and unstable regions) exhibit complex vortex geometries and behaviour and hence, are not considered in the development of Eq. (29). In some cases, a distinct vortex formation behaviour in the near wake is observed. Fig. 12(a) shows a complex formation of vortex shedding at $\beta = 0.4$, $H = 2500$, and $Re_L = 7500$, where the free shear layer separated from the cylinder surface rolls up towards the cylinder. Due to the relatively high free stream velocity, the vorticity is concentrated into vortex sheets on the surface of the vortex, which leads to the development of the irrotational core. Another
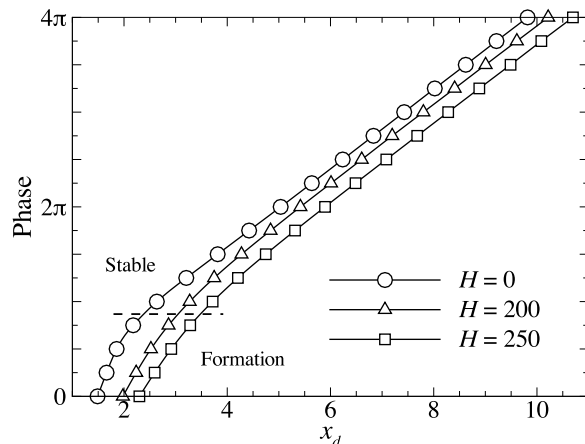

FIG. 10. Phase relationships along the wake for $\beta = 0.1$ and $Re_L = 800$. The dashed line separates the regions of vortex formation and stable wake.
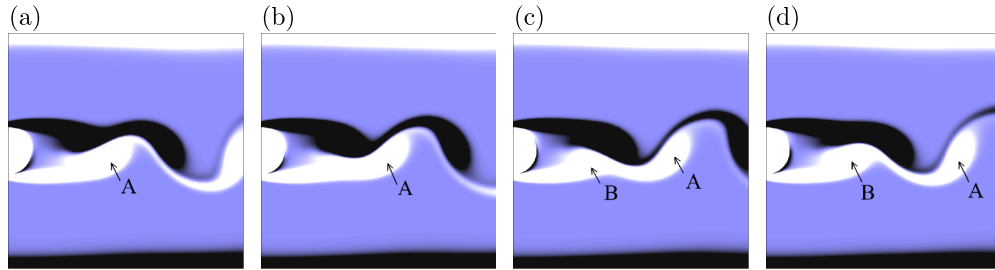
FIG. 11. Typical formation of vortex shedding of a cylinder for $\beta = 0.2$, $H = 500$, and $Re_L = 1500$. Non-dimensional time increment $\Delta t = 0.25$, $T \approx 0.36$ between each subfigure, where T is period. Vorticity contour levels range uniformly from $\xi = -2$ (black) to 2 (white).

interesting feature of the flow is the appearance of a secondary vortex within the recirculation zone. During the vortex sheet roll-up, the primary vortex shedding deforms and eventually is torn apart, giving birth to the secondary vortex. As the vortex propagates downward, the irrotational core shrinks and eventually disappears. Beyond this point of disappearance, the vortex street becomes more coherent and stable. Comparison of the decaying peak vorticity from the current numerical data along with the prediction from Eq. (29) (refer Fig. 12(b)) reveals overprediction towards the cylinder, but becoming more predictable further downstream. The overprediction at the beginning of the vortex shedding is expected due to the fact that part of the fed vorticity is supplied to the secondary vortex. This explains the scatter of data towards the stronger vorticity region seen in Fig. 9. As vortices move further downstream, the wake stabilizes, and hence, Eq. (29) becomes more capable of predicting the peak vorticity, which produces the excellent collapse of data to a straight line of unit gradient as data approaches the origin. The accuracy of the devised model was further assessed by comparing the experimental and numerical results from Kieft *et al.*[54] and Ponta[46] of unbounded channel flows ($\beta = 0$) along with the predictions from Eq. (31) and is plotted in Fig. 13. The predictions compare very well with the numerical results; however, deviation further downstream is seen in the experimental results. Kieft *et al.*[54] attribute this discrepancy to the lower spatial resolution and noise in the experimental measurements.

V. INTERPRETATION OF THE MODEL

Equation (29) provides numerous insights into the spatial evolution of the wake vortices. First, the spatial decay rate of peak vorticity can be predicted. In a similar fashion to the conventional
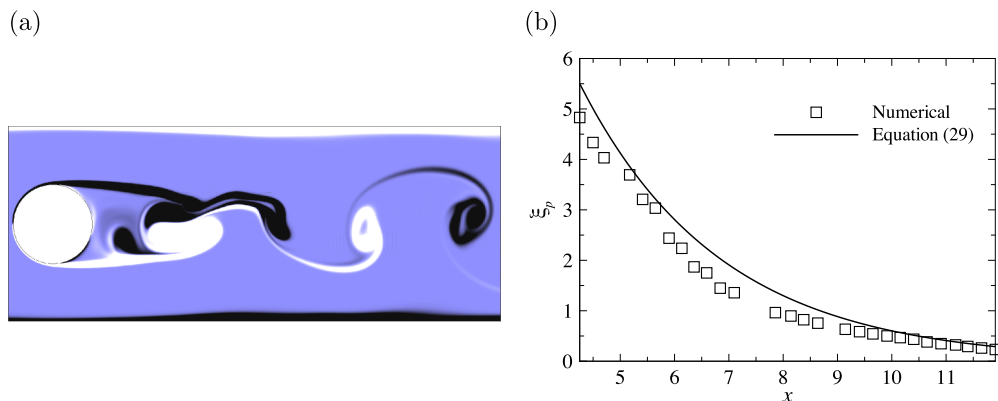

FIG. 12. (a) Instantaneous vorticity contour plots at the formation region and (b) decaying peak vorticity spatial history for the case of $\beta = 0.4$, $H = 2500$, and $Re_L = 7500$. In (a), contour levels are as per Fig. 11. In (b), square symbols represent numerical data and solid line represents prediction by Eq. (29).
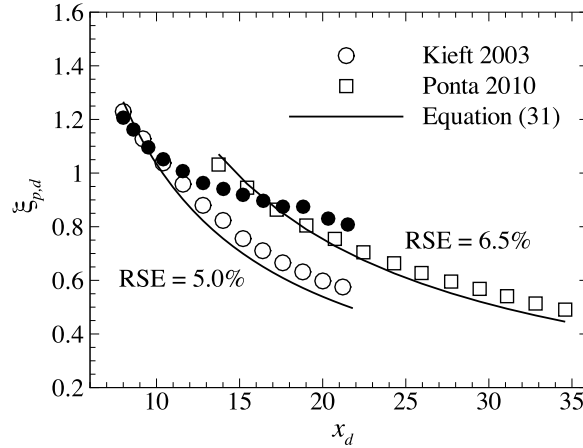
FIG. 13. Comparison of predicted peak vorticity spatial evolution with the previous experimental data[54] and numerical data.[46,54] Open and solid symbols represent numerical data and experimental data, respectively, while lines represent predicted values.

approach for analysing mode evolution using the Stuart–Landau equation,[55,56] a model that provides a tool for the study of the non-linear behaviour near the critical Reynolds number, an "instantaneous" spatial decay rate may be defined as the spatial derivative of the natural logarithm of peak vorticity, which evaluates to

$$\frac{\partial(\log_e \xi_{\perp,p})}{\partial x} = -\frac{1}{x + (0.075\beta + 0.01)Re_d(1-\beta) - (4.3\beta - 0.15)} - 0.90\frac{H}{Re_L^{0.974}}. \qquad (34)$$

As x approaches infinity, the first term on the RHS vanishes, and the instantaneous decay rate reaches an asymptote of $-0.9H/Re_L^{0.974}$. This closely resembles the decay described by the Hartmann friction term in the governing equation (i.e., $-H/Re_L$). This implies that viscosity only contributes to the dissipation of vortices in the near wake; far downstream only Hartmann friction is significant. Furthermore, it can be seen from Fig. 14 that the decay rate is strongly dependent on friction parameter and Reynolds number at their higher and lower ranges, respectively. This can be attributed to the fact that at these ranges, viscous decay becomes less significant and the Hartmann braking effect becomes more prominent. Hence, the decay rate becomes sensitive to the changes in friction parameter. Fig. 14 also implies that lower blockage ratio leads to faster decay of vorticity.
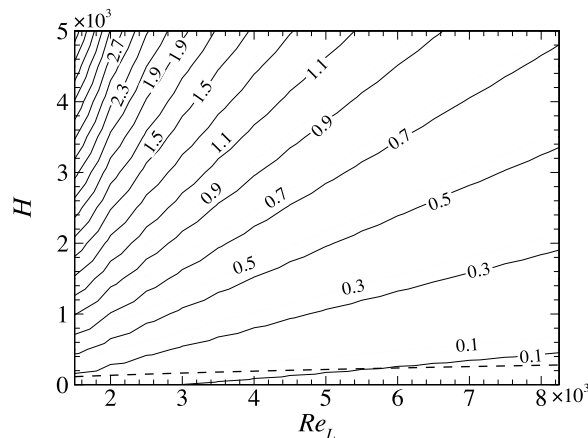

FIG. 14. Contours of the absolute value of the instantaneous spatial decay rate of vorticity against Re_L and H at $x = 1$, determined from Eq. (34). Solid and dotted lines indicate $\beta = 0.1$ and $\beta = 0.4$, respectively. The dashed line indicates the $N = 10$ curve, above which the assumption of SM82 model ($N \gg 1$) is applicable.

Furthermore, recalling the form of the quasi-two-dimensional analogue of the Lamb–Oseen vortex, the right-hand-side terms of Eq. (34) are derived from the hyperbolic and exponential decay components arising from viscous diffusion ($\xi_{p,\text{visc}}$) and Hartmann braking ($\xi_{p,H}$), respectively. For any given flow parameters, both terms will always be negative, i.e., both terms are acting to reduce the intensity of the vortex. To express the relative contributions of each component to the decay of vorticity, the ratio of these terms is evaluated, i.e.,

$$\frac{\partial(\log_e \xi_{p,\text{visc}})}{\partial x} \bigg/ \frac{\partial(\log_e \xi_{p,H})}{\partial x} = \frac{1}{b(x - x_0)}, \tag{35}$$

and is depicted in Fig. 15. A ratio of gradients greater (less) than unity indicates region dominated by viscous dissipation (magnetic damping). It is interesting to note that at low friction parameter, the decay of the wake vortices is first dominated by viscous dissipation, and beyond some critical distance, downstream will be dominated by the magnetic damping, which corroborates the afore-mentioned discussion. It should be qualified that this analysis is derived from quasi-2D simulations, and it is likely that at least some of the predicted viscous-dominated region would see a deviation between quasi-2D and real 3D vortex decays as the scale of the vortex impinges on the limits for quasi-two-dimensionality discussed in Sec. II.

The region for this transition is located where both viscous dissipation and magnetic damping contribute equally to the decay of peak vorticity. It (i.e., the critical location) is found by solving Eq. (35) equal to unity for x, which yields

$$\begin{aligned} x_{\text{crit}} &\approx \left\{ x : \frac{1}{b(x - x_0)} = 1 \right\} \\ &= \frac{Re_L^{0.974}}{0.90H} - (0.075\beta + 0.01)Re_d(1 - \beta) + (4.3\beta - 0.15). \end{aligned} \tag{36}$$

Equation (36) states that for a given Reynolds number, the turning point advances upstream as the friction parameter increases, indicative of a shorter viscous dissipation dominated region (which is also shown in Fig. 15). At a critical friction parameter, the magnetic damping effect already prevails from the beginning of the decay process. In order to validate these model predictions against quasi-two-dimensional simulations, simulations were carried out for hydrodynamic and magneto-hydrodynamic cases. In both cases, simulations are started with the wake at a fully saturated state and under the influence of magnetic field. The flows were then evolved over a very short time interval, and the change in vortex strength of each wake vortex was then used to calculate the local instantaneous decay rate of peak vorticity. The process was repeated for initial conditions at several
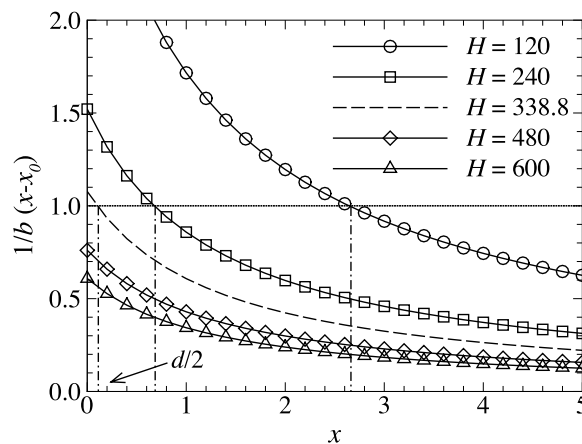

FIG. 15. Spatial history of viscous-to-magnetic damping gradients ratio for $\beta = 0.1$ and $Re_L = 500$. The dotted line indicates the border of magnetic damping dominated region, and the corresponding locations at different Ha are shown by the dashed-dotted lines. The dashed curve indicates the critical H above which Hartmann braking dominates for the entire wake. The expression for parameters b and x_0 is given in Eq. (29), and $d/2$ is the cylinder radius.
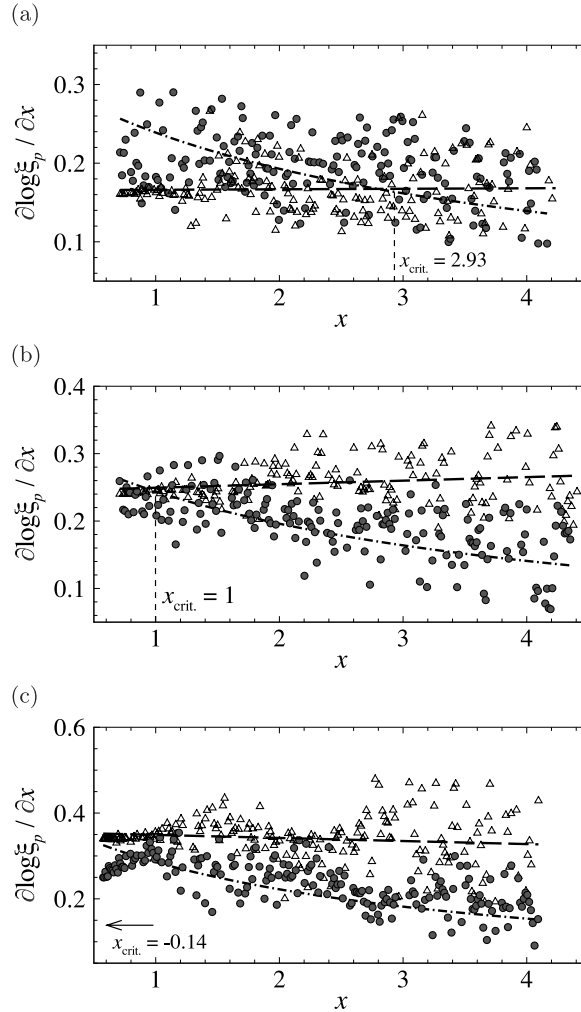
FIG. 16. Local instantaneous rate of peak vortex decay for the case of $\beta = 0.1$, $Re = 1000$, and (a) $H = 160$, (b) $H = 240$, and (c) $H = 340$. Circle and triangle symbols represent decay rate due to viscous dissipation and Hartmann braking, respectively. Dashed and dashed-dotted lines show the regression fits for each data set. Vertical dashed lines in (a) and (b) indicate the crossover locations predicted by Eq. (36).

different phases over a shedding period. The Hartmann braking contribution to the rate of vortex decay was estimated by taking the difference in the rates of decay obtained from both the hydrodynamic (due to viscous dissipation only) and magnetohydrodynamic (due to viscous dissipation and Hartmann braking) cases. It turns out that the data are systematically scattered (as seen in Fig. 16). The data were then fitted to a power law and a linear trend for viscous dissipation and Hartmann braking contributions, respectively, which follows from the form of Eq. (34). The intersection of these curves indicates the critical location at which the viscous dissipation and magnetic damping contributions balance each other out. Figs. 16(a) and 16(b) reveal that the critical locations compare very well with the predictions from Eq. (36), where higher friction parameter tends to move the critical location further upstream. It is also observed in Fig. 16(c) that as friction parameter is increased above the critical value, the fitted curves do not intersect downstream of the cylinder, consistent with Hartmann braking dominating throughout the wake. The model therefore not only predicts the overall quasi-two-dimensional wake vortex decay but also accurately describes the physical contributions of Hartmann braking and viscous dissipation towards the decay process.

The critical friction parameter (i.e., the minimum friction parameter at which the decay is dominated by the magnetic damping only) is evaluated by solving $x_{\text{crit}} = x_{\text{decay}}$ for H, where x_{decay} is the location of the beginning of the decay process. If the decay of vorticity is taken to begin at

the rear of the cylinder, i.e., at $x = d/2 = \beta L$, and noting that $Re_d = 2\beta Re_L$, then the critical friction parameter is given by

$$H_{\text{crit}} = \frac{Re_L^{0.974}}{0.90(\beta L + 2\beta(0.075\beta + 0.01)Re_L(1 - \beta) - (4.3\beta - 0.15))}. \tag{37}$$

This critical friction parameter is mapped against Reynolds number and blockage ratio, as shown in Fig. 17. The main observation inferred from Fig. 17 is that Hartmann braking dominates the decay of vorticity at higher blockage ratio and higher Reynolds number, which is in agreement with the previous findings.[8] The effect of blockage ratio and Reynolds number on the predominancy of Hartmann braking is more prominent at their lower ranges (i.e., $\beta \lesssim 0.2$ and $Re_L \lesssim 1000$). Furthermore, at higher Re_L, the critical friction parameter becomes almost independent of Reynolds number for any given blockage ratio. This observation is attributed to the asymptotic behaviour of Eq. (35) for large values of Reynolds number, i.e., $1/b(x - x_0) \approx H^{-1}Re/(x + Re) \sim H^{-1}$ for $x \ll Re$.

As mentioned in Sec. IV, the SM82 model is valid when $N \gg (a/l_\perp)^3$ and $H \gg (a/l_\perp)^2$. Fig. 17 suggests that for cases where the combination of β and Re_L lies in the $N_{\text{crit}} > 10$ region, it is possible to have quasi-two-dimensional MHD flow with vortices dominated by viscous decay for part of their lifetime in the wake provided that restriction on the perpendicular length scale is still satisfied. However, under the SM82 model, the momentum at the vicinity of the Hartmann layer is assumed to diffuse immediately due to the Joule dissipation time τ_{2D} being much less than the time scales for viscous diffusion in the perpendicular plane, $\tau_\nu^\perp$.[29,57] As a result, the SM82 model breaks down locally when the effect of viscosity is relevant, i.e., when $Ha \sim l_\parallel/l_\perp$, or when the transverse length scale $l_\perp$ is of the order of the Shercliff layers thickness, $\delta_S = aHa^{-1/2}$. Despite the inherent limitations of the SM82 model, it has nevertheless been shown to predict the Shercliff layers thickness and an isolated vortex profile to high accuracy when compared to 3D solutions,[36] where the reported errors are less than 10%.[29,38] The model has also been tested for flows in a duct with a cylinder obstacle, where the critical Reynolds number at the onset of vortex shedding in Refs. 8 and 38 compares well with the 3D direct numerical simulation results[26] and experimental results.[25] Furthermore, Kanaris *et al.*[26] found that the critical Reynolds number decreases as *Ha* is increased at a low Hartmann number (i.e., $Ha \lesssim 35$, corresponding to $N \lesssim 2$). However, critical Reynolds number varies almost linearly with Hartmann number for higher Hartmann number, which is in agreement with the previous findings.[8,25,26,38] Surprisingly, this non-monotonic trend is also observed in a wake-type vortex using the SM82 model.[15] This observation is supported by more recent findings,[27] where the transition to two-dimensionality of wake vortices occurs at relatively low interaction parameter ($1 < N < 5$). It is hence anticipated that the SM82 model will be able to provide some
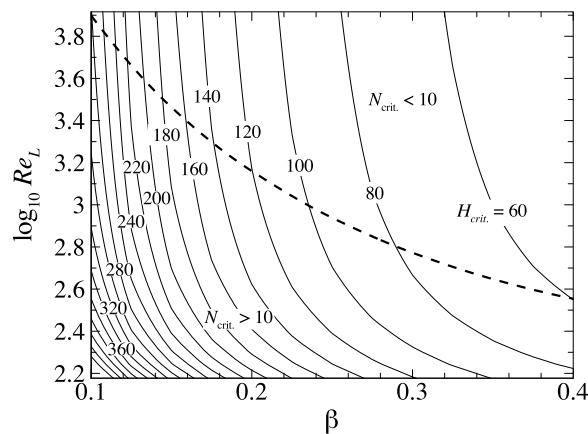

FIG. 17. Contour mapping of H_{crit} over the β-$\log_{10} Re_L$ parameter space. The dashed line shows a curve of $N_{\text{crit}} = H_{\text{crit}}^2/Re_L = 10$. If N_{crit} exceeds the interaction parameter required for validity of the SM82 model (here representatively as $N = 10$), then it may be possible that a quasi-2D wake vortex experiencing viscous-dominated decay for some of its lifetime.

trustworthy insights into the two-dimensional wake behaviour beyond the parameter ranges where it is formally applicable. Moreover, the requirement for the analytical threshold vortex size presented in Sec. II is stricter than that of perpendicular scales. This suggest that at least some of the wakes produced for $H < H_{crit}$ will formally satisfy the SM82 model. These arguments support the application of the wake vortex decay model developed in this study to wakes across a wide range of Re and H, including cases where viscous diffusion contributes more significantly than Hartman braking to the vortex decay for at least part of their lifetime. Fig. 17 also suggest that at higher Reynolds numbers (where the combination of β and Re_L lies in the $N_{crit} < 10$ region), the decay of quasi-two-dimensional MHD wake vortices must always be dominated by Hartmann braking for the entire wake. This is because in this region, H_{crit} is lower than the friction parameter required to produce interaction parameter satisfying quasi-two-dimensionality. This supports the conjecture that quasi-2D MHD turbulence is dominated by Hartmann braking in this region.[58]
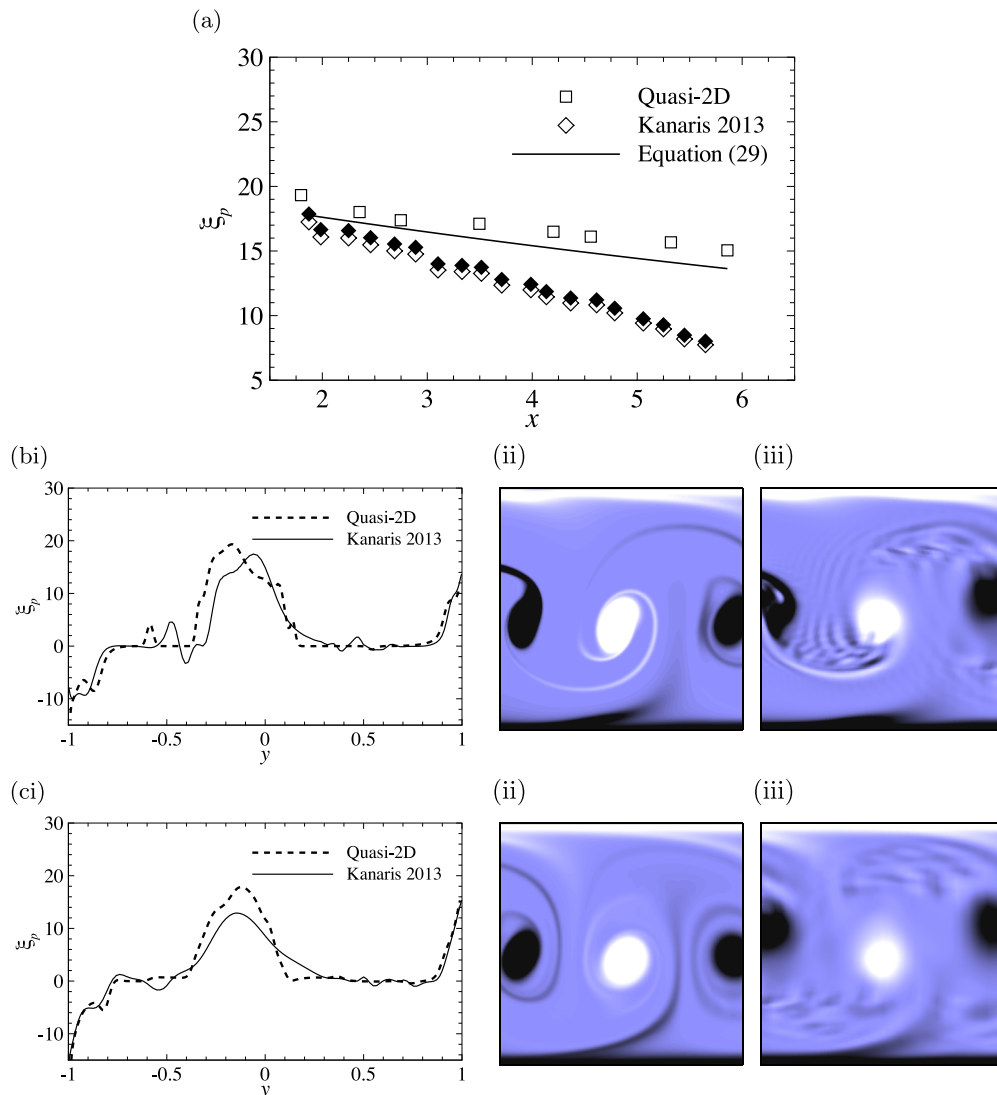

FIG. 18. Case $U1$: $\beta = 0.25$, $H = 160$, $Re_L = 4000$, and $N = 6.4$. (a) Peak vorticity spatial evolution. Square and diamond (open) symbols represent data from present quasi-2D simulations and previous 3D numerical results.[26] Solid symbols are 3D data normalized to Eq. (29) prediction at the first vortex location and solid line represents predicted values. (bi) Vorticity profiles in the transverse direction at $x = 1.8$. (bii) and (biii) Instantaneous vorticity contour plot from the present quasi-2D and previous 3D simulations,[26] respectively. Contour levels are as per Fig. 11. (ci)-(ciii) Captions as per (bi)-(biii), respectively, at $x = 3.6$.

VI. COMPARISON WITH THREE-DIMENSIONAL DATA AT LOW AND MODERATE INTERACTION PARAMETERS

In this section, the predicted peak vorticity from the current model is compared to recently computed three-dimensional direct numerical simulations by Kanaris *et al.*[26] Three cases are compared, namely, cases $U1$, $U2$, and $U3$ having interaction parameters $N_d \approx 3.2$, $N_d \approx 1.3$, and $N_d \approx 15.7$, respectively. N_d is the interaction parameter based on cylinder diameter, and these correspond to our interaction parameter based on duct height with values $N = H^2/Re_L \approx 6.4$, $N \approx 2.6$, and $N \approx 31.4$ for cases $U1$, $U2$, and $U3$, respectively. The aim here is to compare the decay rate of wake vortices in quasi-2D MHD flows against the corresponding three-dimensional flows at low and moderate interaction parameters.

First, a comparison of case $U1$ is considered. Fig. 18(a) compares the spatial evolution of peak vortex strength from 3D data of Kanaris *et al.*,[26] taken at the middle plane, present quasi-2D simulations and present model predictions, noting that the peak vorticity is potentially a very sensitive measure of a vortex strength. A normalization of the 3D data is also plotted to provide a better comparison in terms of the rate of vortex decay with the model predictions. The predictions compare very well with the 3D data in the near wake region, but the wake decays faster further downstream in the presence of three-dimensionality. However, inspection of vortex profiles at arbitrary locations reveals that the breadth of the vortex from both quasi-2D and 3D simulations is comparable, as shown in Figs. 18(bi)–18(ciii). It is also interesting to note from Figs. 18(bi) and 18(ci) that the Shercliff layers' thickness in the quasi-2D and 3D simulations is in a very good agreement, confirming previous findings.[29]

In case $U2$, there is poor agreement between quasi-2D and 3D peak vorticity spatial histories, as shown in Fig. 19(a). This is expected because at this low interaction parameter, the near wake is highly three-dimensional,[26] and the SM82 model is certainly inaccurate. Furthermore, recent experimental investigation by Rhoads, Edlund, and Ji[59] found that at low interaction parameter, the evolution of wake vortices was significantly altered due to the prevalence of small-scale turbulent eddies, which corroborates the aforementioned argument. Inspection of Figs. 19(bi)–19(biii) reveals
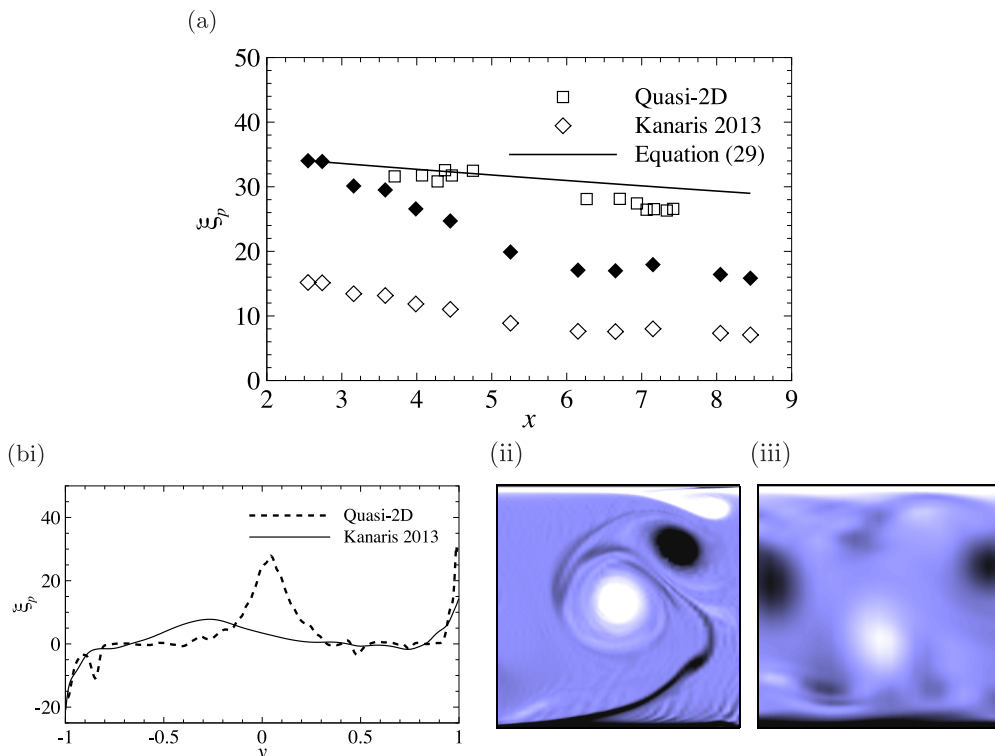

FIG. 19. Case $U2$: $\beta = 0.25$, $H = 160$, $Re_L = 10\,000$ and $N = 2.6$. Captions are as per Fig. 18, (bi)-(biii) $x = 6.7$.

that the vorticity profile from 3D simulations is almost uniform, most likely due to diffusion of vorticity in the magnetic field direction. However, the rate of peak vorticity decay is in good agreement further downstream. This observation can be attributed to the transition to a two-dimensional state, as discussed by Mück *et al.*[27] In their 3D simulations at a low interaction parameter ($N_d = 1$), they observed that the spanwise velocity fluctuation tends to zero farther from the cylinder and that the vorticity diffuses along the magnetic field lines, an evidence of two-dimensionality.

Comparisons of decaying peak vorticity for case $U3$ are shown in Fig. 20(a). Having the highest N, this case is expected to produce the best agreement. It can be seen that quasi-2D model tends to overpredict the intensity of wake vortices, seemingly due to different wake vortex profiles. As depicted in Fig. 20(bi), the vortex produced by the 3D simulations resembles a Rankine vortex with solid body rotation in the core region, whereas the vortex in the quasi-2D model exhibits a Lamb–Oseen vortex. The corresponding contour plots of these vortices are shown in Figs. 20(bii) and 20(biii). Figs. 20(ci)–20(ciii) show vorticity profiles and the corresponding contour plots at a further downstream location. Despite the overprediction of the vortex strength, the proposed model seems to perform very well at predicting the rate of vorticity decay, where the normalized 3D data almost coincide with the predicted line plot (refer Fig. 20(a)).
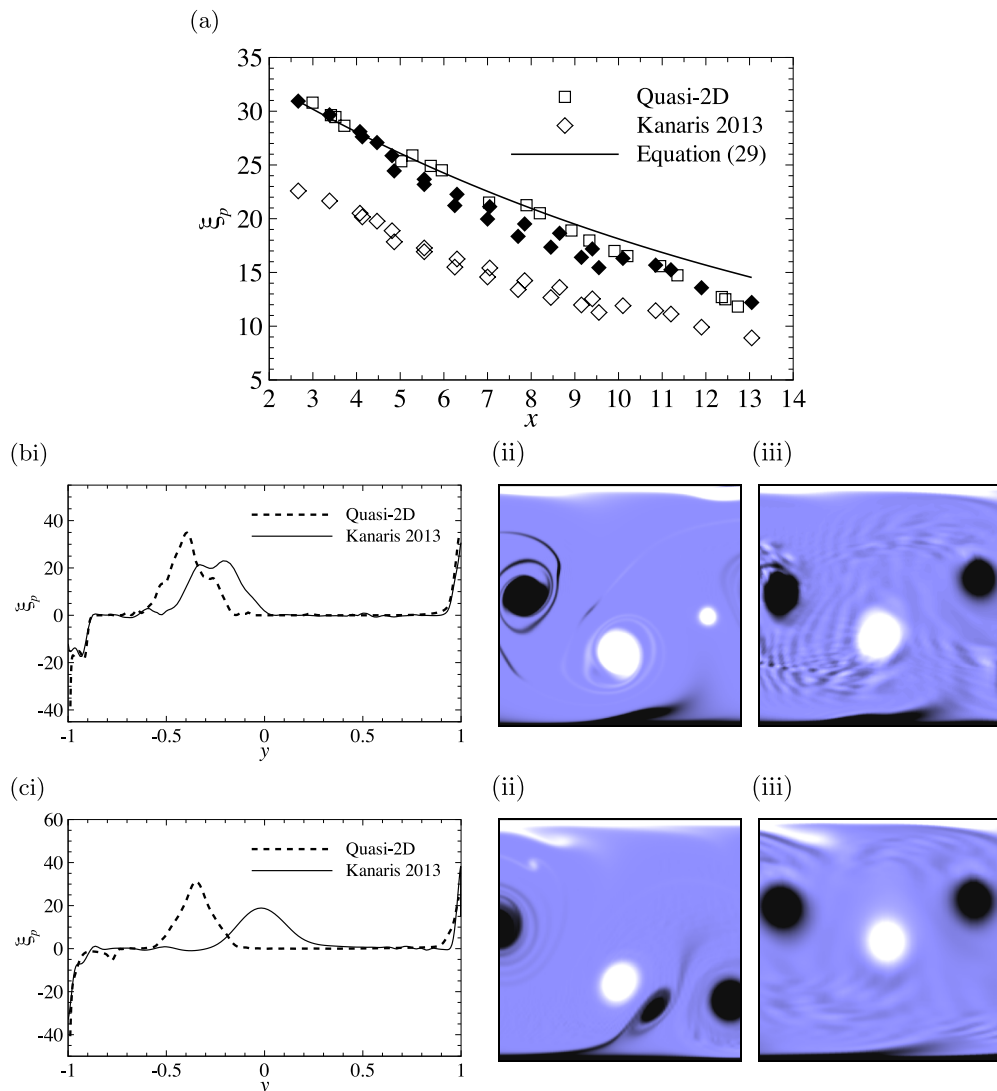

FIG. 20. Case $U3$: $\beta = 0.25$, $H = 560$, $Re_L = 10\,000$, and $N = 31.4$. Captions are as per Fig. 18, (bi)-(biii) $x = 2.2$, and (ci)-(ciii) $x = 4.5$.

VII. CONCLUSION

The present study investigates the decay behaviour of a stable wake vortices behind a circular cylinder under the influence of a strong magnetic field parallel to the cylinder axis. Under these conditions, the velocity field becomes almost independent of the spanwise direction in the bulk and hence, is treated as quasi-two-dimensional flow. The numerical simulations have been performed over the range of blockage ratios $0.1 \le \beta \le 0.4$, friction parameter $500 \le H \le 5000$, and Reynolds numbers $300 \le Re_L \le 8250$.

The analytical solution for the decay of a quasi-two-dimensional MHD vortex is obtained, and this forms the basis for a regression fit to describe the decay of stable wake vortices behind an idealized turbulence promoter (i.e., a circular cylinder) in a rectangular duct. The devised model proposes that the decay rate varies with blockage ratio, imposed magnetic field intensity, and Reynolds number. This model can further describe hydrodynamic vortex decay ($H = 0$) and decay of wake vortices in an open flow ($\beta = 0$). The instantaneous spatial decay rate becomes sensitive to the change in friction parameter and Reynolds number at their higher and lower ranges, respectively. As vortices are advected far downstream, the decay rate approaches an approximate Hartmann friction term (i.e., $-H/Re_L$).

The model also predicts that quasi-two-dimensional vortices can be dominated by viscous decay in the near wake, if the friction parameter remains below a critical value. Friction parameters lower than this critical value imply that there are two distinct regions of dominant decay forcing, i.e., viscous dissipation in the near wake and Hartmann braking further downstream. Otherwise, Hartman braking dominates the decay for the entire wake. The critical friction parameter is dependent on Reynolds number and blockage ratio, where higher Re_L and β lead to lower H_{crit}. However, the critical friction parameter becomes almost constant for a higher level of flow turbulence due to the counterbalancing effects of both viscous dissipation and Hartmann braking. Under this condition, the quasi-two-dimensional MHD vortex decay is dominated by Hartmann braking. Furthermore, this dependency becomes more apparent at lower Re_L and β.

A comparison between the model predictions and published 3D MHD simulation data at different interaction parameters confirms the capability of the proposed model in predicting the rate of peak vorticity decay within an advecting vortex at high interaction parameters.

In the present study, the model was developed using wake data in a laminar regime. Nevertheless, quasi-2D MHD turbulence is of great importance to physical engineering problems and has been the subject of interest over the past several decades. The decay behaviour of a cylinder wake vortices in the transient and turbulent environments would be an interesting topic for investigation in the future.

[1] J. Sommeria and R. Moreau, "Why, how, and when, MHD turbulence becomes two-dimensional," J. Fluid Mech. **118**, 507–518 (1982).

[2] P. J. Dellar, "Quasi-two-dimensional liquid–metal magnetohydrodynamics and the anticipated vorticity method," J. Fluid Mech. **515**, 197–232 (2004).

[3] Z. Hussain, L. Chan, Z. Nianmei, and N. Mingjiu, "Instability in three-dimensional magnetohydrodynamic flows of an electrically conducting fluid," Plasma Sci. Technol. **15**, 1263 (2013).

[4] Y. B. Kolesnikov and O. V. Andreev, "Heat-transfer intensification promoted by vortical structures in closed channel under magnetic field," Exp. Therm. Fluid Sci. **15**, 82–90 (1997).

[5] G. Mutschke, G. Gerbeth, V. Shatrov, and A. Tomboulides, "Two-and three-dimensional instabilities of the cylinder wake in an aligned magnetic field," Phys. Fluids **9**, 3114–3116 (1997).

[6] G. Mutschke, V. Shatrov, and G. Gerbeth, "Cylinder wake control by magnetic fields in liquid metal flows," Exp. Therm. Fluid Sci. **16**, 92–99 (1998).

[7] H. S. Yoon, H. H. Chun, M. Y. Ha, and H. G. Lee, "A numerical study on the fluid flow and heat transfer around a circular cylinder in an aligned magnetic field," Int. J. Heat Mass Transfer **47**, 4075–4087 (2004).

[8] W. K. Hussam, M. C. Thompson, and G. J. Sheard, "Dynamics and heat transfer in a quasi-two-dimensional MHD flow past a circular cylinder in a duct at high Hartmann number," Int. J. Heat Mass Transfer **54**, 1091–1100 (2011).

[9] H. Branover, A. Eidelman, and M. Nagorny, "Use of turbulence modification for heat transfer enhancement in liquid metal blankets," Fusion Eng. Des. **27**, 719–724 (1995).

[10] H. Huang and B. Li, "Heat transfer enhancement of free surface MHD-flow by a protrusion wall," Fusion Eng. Des. **85**, 1496–1502 (2010).

[11] S. Cuevas, S. Smolentsev, and M. A. Abdou, "On the flow past a magnetic obstacle," J. Fluid Mech. **553**, 227–252 (2006).

[12] E. V. Votyakov, E. Zienicke, and Y. B. Kolesnikov, "Constrained flow around a magnetic obstacle," J. Fluid Mech. **610**, 131–156 (2008).

[13] S. Kenjereš, S. ten Cate, and C. J. Voesenek, "Vortical structures and turbulent bursts behind magnetic obstacles in transitional flow regimes," Int. J. Heat Fluid Flow **32**, 510–528 (2011).

[14] S. Kenjereš, "Energy spectra and turbulence generation in the wake of magnetic obstacles," Phys. Fluids **24**, 115111 (2012).

[15] L. Bühler, "Instabilities in quasi-two-dimensional magnetohydrodynamic flows," J. Fluid Mech. **326**, 125–150 (1996).

[16] J. Sommeria, "Electrically driven vortices in a strong magnetic field," J. Fluid Mech. **189**, 553–569 (1988).

[17] T. Alboussière, V. Uspenski, and R. Moreau, "Quasi-2D MHD turbulent shear layers," Exp. Therm. Fluid Sci. **20**, 19–24 (1999).

[18] A. Pothérat and R. Klein, "Why, how and when MHD turbulence at low *Rm* becomes three-dimensional," J. Fluid Mech. **761**, 168–205 (2014).

[19] S. Taneda, "Experimental investigation of the wakes behind cylinders and plates at low Reynolds numbers," J. Phys. Soc. Jpn. **11**, 302–307 (1956).

[20] M. Gaster, "Vortex shedding from slender cones at low Reynolds numbers," J. Fluid Mech. **38**, 565–576 (1969).

[21] J. H. Gerrard, "The wakes of cylindrical bluff bodies at low Reynolds number," Philos. Trans. R. Soc., A **288**, 351–382 (1978).

[22] H. Lamb, *Hydrodynamics* (Cambridge University Press, 1932).

[23] K. P. Chopra and L. F. Hubert, "Kármán vortex streets in wakes of islands," AIAA J. **3**, 1941–1943 (1965).

[24] P. A. Davidson, "The role of angular momentum in the magnetic damping of turbulence," J. Fluid Mech. **336**, 123–150 (1997).

[25] M. Frank, L. Barleon, and U. Müller, "Visual analysis of two-dimensional magnetohydrodynamics," Phys. Fluids **13**, 2287 (2001).

[26] N. Kanaris, X. Albets, D. Grigoriadis, and S. Kassinos, "Three-dimensional numerical simulations of magnetohydrodynamic flow around a confined circular cylinder under low, moderate, and strong magnetic fields," Phys. Fluids **25**, 074102 (2013).

[27] B. Mück, C. Günther, U. Müller, and L. Bühler, "Three-dimensional MHD flows in rectangular ducts with internal obstacles," J. Fluid Mech. **418**, 265–295 (2000).

[28] C. W. Oseen, "Über wirbelbewegung in einer reiben den flüssigkeit," Ark. J. Mat. Astron. Fys. **7**, 14–21 (1912).

[29] A. Pothérat, "Quasi-two-dimensional perturbations in duct flows under transverse magnetic field," Phys. Fluids **19**, 074104 (2007).

[30] A. D. Polyanin, *Handbook of Linear Partial Differential Equations for Engineers and Scientists* (CRC Press, 2010).

[31] P. G. Saffman, *Vortex Dynamics* (Cambridge University Press, 1992).

[32] W. W. Durgin and S. K. F. Karlsson, "On the phenomenon of vortex street breakdown," J. Fluid Mech. **48**, 507–527 (1971).

[33] J. C. McWilliams, "The vortices of two-dimensional turbulence," J. Fluid Mech. **219**, 361–385 (1990).

[34] M. Sahin and R. G. Owens, "A numerical investigation of wall effects up to high blockage ratios on two-dimensional flow past a confined circular cylinder," Phys. Fluids **16**, 1305–1320 (2004).

[35] W. J. Devenport, M. C. Rife, S. I. Liapis, and G. J. Follin, "The structure and development of a wing-tip vortex," J. Fluid Mech. **312**, 67–106 (1996).

[36] A. Pothérat, J. Sommeria, and R. Moreau, "An effective two-dimensional model for MHD flows with transverse magnetic field," J. Fluid Mech. **424**, 75–100 (2000).

[37] A. Pothérat, J. Sommeria, and R. Moreau, "Numerical simulations of an effective two-dimensional model for flows with a transverse magnetic field," J. Fluid Mech. **534**, 115–143 (2005).

[38] V. Dousset and A. Pothérat, "Numerical simulations of a cylinder wake under a strong axial magnetic field," Phys. Fluids **20**, 017104 (2008).

[39] D. Krasnov, O. Zikanov, and T. Boeck, "Numerical study of magnetohydrodynamic duct flow at high Reynolds and Hartmann numbers," J. Fluid Mech. **704**, 421 (2012).

[40] W. K. Hussam, M. C. Thompson, and G. J. Sheard, "Enhancing heat transfer in a high Hartmann number magnetohydrodynamic channel flow via torsional oscillation of a cylindrical obstacle," Phys. Fluids **24**, 113601 (2012).

[41] W. K. Hussam, M. C. Thompson, and G. J. Sheard, "Optimal transient disturbances behind a circular cylinder in a quasi-two-dimensional magnetohydrodynamic duct flow," Phys. Fluids **24**, 024105 (2012).

[42] A. Roshko, "On the development of turbulent wakes from vortex streets," Technical Report No. 1191 (National Advisory Committee for Aeronautics, 1954).

[43] C. H. K. Williamson, "Oblique and parallel modes of vortex shedding in the wake of a circular cylinder at low Reynolds numbers," J. Fluid Mech. **206**, 579–627 (1989).

[44] W. K. Hussam and G. J. Sheard, "Heat transfer in a high Hartmann number MHD duct flow with a circular cylinder placed near the heated side-wall," Int. J. Heat Mass Transfer **67**, 944–954 (2013).

[45] A. Pothérat, J. Sommeria, and R. Moreau, "Effective boundary conditions for magnetohydrodynamic flows with thin Hartmann layers," Phys. Fluids **14**, 403 (2002).

[46] F. L. Ponta, "Vortex decay in the Kármán eddy street," Phys. Fluids **22**, 093601 (2010).

[47] A. Pothérat and J.-P. Schweitzer, "A shallow water model for magnetohydrodynamic flows with turbulent Hartmann layers," Phys. Fluids **23**, 055108 (2011).

[48] R. Kieft, "Mixed convection behind a heated cylinder," Ph.D. thesis (Technische Universiteit Eindhoven, 2000).

[49] M. Goodarzi, P. Shahbazikhah, M. R. Sohrabi, M. Fathabadi, and S. H. Nouri, "Direct orthogonal signal correction-partial least squares for simultaneous spectrophotometric determination of sulfamethoxazole and trimethoprim in pharmaceutical formulation and synthetic samples," J. Chil. Chem. Soc. **54**, 309–313 (2009).

[50] K. Asadpour-Zeynali and S. Manafi-Khoshmanesh, "Simultaneous standard addition method for novel determination of components in a single step: Application in analysis of sunset yellow and carmoisine by a spectrophotometric technique," Anal. Methods **6**, 6110–6115 (2014).

[51] R. J. Klein, S. E. Proctor, M. A. Boudreault, and K. M. Turczyn, "Healthy people 2010 criteria for data suppression," Stat. Notes **24**, 1–12 (2002).

[52] J. W. Schaefer and S. Eskinazi, "An analysis of the vortex street generated in a viscous fluid," Ph.D. thesis (Cambridge University Press, 1958).

[53] P. W. Bearman, "On vortex street wakes," J. Fluid Mech. **28**, 625–641 (1967).

[54] R. N. Kieft, C. C. M. Rindt, A. A. Van Steenhoven, and G. J. F. Van Heijst, "On the wake structure behind a heated horizontal cylinder in cross-flow," J. Fluid Mech. **486**, 189–211 (2003).

[55] G. J. Sheard, M. C. Thompson, and K. Hourigan, "Asymmetric structure and non-linear transition behaviour of the wakes of toroidal bodies," Eur. J. Mech. B/Fluids **23**, 167–179 (2004).

[56] G. J. Sheard, M. C. Thompson, and K. Hourigan, "From spheres to circular cylinders: Non-axisymmetric transitions in the flow past rings," J. Fluid Mech. **506**, 45–78 (2004).

[57] V. Dousset, "Numerical simulations of MHD flows past obstacles in a duct under externally applied magnetic field," Ph.D. thesis (Coventry University, 2009).

[58] A. Pothérat, "Low *Rm* MHD turbulence: The role of boundaries," *8th PAMIR International Conference on Fundamental MHD and Liquid Metal Technology*, Borgo Corsica, France, September 5-9, 2011, Magnetohydrodynamics **48**, 13–23 (2012).

[59] J. R. Rhoads, E. M. Edlund, and H. Ji, "Effects of magnetic field on the turbulent wake of a cylinder in free-surface magnetohydrodynamic channel flow," J. Fluid Mech. **742**, 446–465 (2014).